Journal of Materials Chemistry A

Efficient near-infrared emission from lead-free ytterbium-doped cesium bismuth halide perovskites

Journal:	*Journal of Materials Chemistry A*
Manuscript ID	TA-ART-03-2021-002147.R1
Article Type:	Paper
Date Submitted by the Author:	05-May-2021
Complete List of Authors:	Tran, Minh; New York University Tandon School of Engineering, Chemical and Biomolecaulr Engineering Department Cleveland, Iver; New York University Tandon School of Engineering, Chemical and Biomolecaulr Engineering Pustorino, Gregory; New York University Tandon School of Engineering, Chemical and Biomolecaulr Engineering Department Aydil, Eray; New York University Tandon School of Engineering, Department of Chemical Engineering and Biomolecular Engineering

ARTICLE

Efficient near-infrared emission from lead-free ytterbium-doped cesium bismuth halide perovskites†

Received 00th January 20xx,
Accepted 00th January 20xx

DOI: 10.1039/x0xx00000x

Minh N. Tran,[a] Iver J. Cleveland,[a] Gregory A. Pustorino,[a] and Eray S. Aydil*[a]

Bismuth-based halide perovskites are non-toxic alternatives to widely researched lead-containing halide perovskites for optoelectronics. Cesium bismuth bromide, in particular, may have good optical properties, but photoluminescence data reported to date are confusing and contradictory. Here we resolve the literature discrepancies and show that $Cs_3Bi_2Br_9$ thin films deposited by physical vapor deposition show absorption and emission peaks at 433 and 472 nm, respectively. Peak location and lineshapes of blue-shifted (390-440 nm) photoluminescence previously reported and attributed to quantum confinement in $Cs_3Bi_2Br_9$ nanocrystal dispersions could be reproduced in $BiBr_3$ solutions in different solvents but without $Cs_3Bi_2Br_9$ nanocrystals present. This suggests that high quantum yield photoluminescence reported in this wavelength range may be originating from unreacted precursors and impurities in nanocrystal dispersions rather than from $Cs_3Bi_2Br_9$ quantum dots. The addition of Yb that can substitute up to 50% of the Bi in $Cs_3Bi_2Br_9$ leaves the $Cs_3Bi_2Br_9$ structure unchanged and results in near-infrared Yb^{3+} $^2F_{5/2}\rightarrow$ $^2F_{7/2}$ emission (1.25 eV) with 14.5% quantum yield. This emission decreases sharply when the perovskite host's bandgap is reduced below 2.5 eV, twice the Yb^{3+} emission energy, by substituting bromine with iodine, raising the possibility that the emission mechanism involves quantum cutting. This would make lead-free $Cs_3Bi_2Br_9$ a potential quantum cutting material for solar spectrum shaping to increase solar cell efficiency.

Introduction

All-inorganic metal halide perovskites have attracted significant attention for solar cells, light-emitting diodes, and photodetectors because they have strong and tunable absorptions and emissions.[1-10] Lead-based perovskites have been the focus of many studies because they perform well in these applications, but lead is toxic. Bismuth-based perovskites are attractive alternatives because bismuth is non-toxic.[11,12] For instance, $Cs_3Bi_2Br_9$ has a high absorption coefficient, and its bandgap is tunable across the entire visible range of the electromagnetic spectrum by substituting Br with Cl or I.[13-15] $Cs_3Bi_2Br_9$ has been studied since the early 1980s and is well known to crystalize in a stable trigonal structure ($P\bar{3}m1, \#164$) at room temperature, which transforms to a monoclinic phase (*C12/c1*, #15) when cooled below 96 K.[16-19] Published optical absorption and photoluminescence (PL) spectra for $Cs_3Bi_2Br_9$, however, vary from article to article.[13,14] Recently, we showed that the literature discrepancies in the optical absorption of $Cs_3Bi_2Br_9$ are due to absorption by $[BiBr_6]^{3-}$ octahedra in Cs_3BiBr_6 phase impurities and by dissolved $[BiBr_6]^{3-}$ ions in colloidal dispersions. Remarkably, absorptions of dissolved $[BiBr_6]^{3-}$ ions and $[BiBr_6]^{3-}$ octahedra in solid Cs_3BiBr_6 peak nearly at the same wavelength (≈383 nm), and they may be easily (and have been) misinterpreted as originating from $Cs_3Bi_2Br_9$. In fact, the $Cs_3Bi_2Br_9$ absorption begins to rise at ≈2.6 eV (470 nm), peaks at ≈2.86 eV (433 nm), drops to a local minimum at ≈3.2 eV (380 nm) and rises again. This peak also originates from $[BiBr_6]^{3-}$ octahedra interacting via corner-sharing in $Cs_3Bi_2Br_9$ to form a narrow excitonic band red-shifted from the absorption of an isolated $[BiBr_6]^{3-}$.

The bandgap of $Cs_3Bi_2Br_9$ and the isovalency of Yb^{3+} with Bi^{3+} makes it a potential host material for quantum cutting, a process wherein photons absorbed at high energies (*e.g.,* > 2.5 eV) generate two photons with energies 1.25 eV via the $^2F_{5/2}\rightarrow$ $^2F_{7/2}$ transition in Yb^{3+}. This transition is close to the silicon bandgap energy (1.1 eV), raising the prospects of a non-toxic, sustainable material that can be deposited as a film on top of a silicon solar cell to increase its efficiency by modifying the solar spectrum. Creating two near-infrared (NIR) photons from a blue or an ultraviolet photon increases the solar cell efficiency by reducing heat generation losses. Recently, Yb-doped $CsPbCl_xBr_{3-x}$ nanocrystals (NC) synthesized using colloidal synthesis have achieved NIR PL quantum yields (PLQY) between 90 and 190%.[20-24] However, quantum yield drops at the highest light intensities, and this material contains the toxic element Pb. Lead-free Yb-doped perovskites, in contrast, show low PLQYs, for instance, ≈ 3% for Yb-doped, $Cs_2AgInCl_6$.[25,26] Both physical vapor deposition (PVD) and solution synthesis have been used to make these Yb doped halide perovskites. PVD and solution synthesis each have their advantages and drawbacks. Most reports utilize solution synthesis, which can be inexpensive, simple, and in some cases can be done at low temperatures.[24]

[a]Department of Chemical and Biomolecular Engineering, Tandon School of Engineering, New York University, New York, New York 11201, USA.
E-mail: aydil@nyu.edu

†Electronic Supplementary Information (ESI) available: Details of PLQY measurements and calculations, additional luminescence spectra from $BiBr_3$ and OA solutions.

However, doping from solution is challenging because of the poor solubility of Yb precursors. Additionally, the structural diversity of the cesium bismuth bromide system, the material of interest in this article, poses challenges to synthesize phase pure $Cs_3Bi_2Br_9$. PVD is a solvent-free technique that provides the means to control precursor fluxes and thus film composition accurately. We take advantage of the PVD method to synthesize phase pure $Cs_3Bi_2Br_9$ films and introduce different amounts of ytterbium into the perovskite host.

Herein, we first address the discrepancies in the visible PL published for $Cs_3Bi_2Br_9$ and show that the high UV-visible-PLQY may not be from $Cs_3Bi_2Br_9$ but may be originating from impurities in colloidal dispersions. We then report Yb-doped $Cs_3Bi_2Br_9$ thin films deposited using PVD with a 14.5% near-infrared PLQY. We could incorporate Yb up to an amount that corresponds to 50% of the Bi sites without disrupting the trigonal structure of $Cs_3Bi_2Br_9$. Moreover, we show that the NIR PLQY decreases sharply when the perovskite host's bandgap is reduced below 2.5 eV, twice the Yb^{3+} emission energy, by substituting iodine into bromine sites. This raises the possibility that the down-conversion is via quantum cutting, making $Cs_3Bi_2Br_9$ a candidate quantum cutting material for solar spectrum shaping to increase solar cell efficiency.

Review of published $Cs_3Bi_2Br_9$ photoluminescence

Wavelengths of published $Cs_3Bi_2Br_9$ UV-visible PL peaks vary significantly, from 389 to 478 nm (Fig. 1). While we may expect blue shifts due to quantum confinement in nanocrystals (*i.e.*, quantum dots, QDs), there are no clear trends in published data where the wavelength decreases with decreasing $Cs_3Bi_2Br_9$ nanocrystal size.

Timmermans and Blasse reported the first PL data for $Cs_3Bi_2Br_9$ single-crystals (SC), two very sharp peaks at 459.2 nm (2.70 eV) and 461.7 nm (2.685 eV) and a broad emission peaking at 476 nm (2.61 eV). (Fig. 1).[16,17] They assigned the sharp 459.2 nm peak to free exciton recombination and hypothesized that the 476 nm line is emission from excitons trapped and localized by Bi^{3+} cation disorder. They also reasoned that the 461.7 nm emission is from a defect that resides at or near the crystals' surfaces because powdering the crystal increased this emission enormously. Room temperature PL from single crystals grown by Leng *et al.* similarly shows a peak at ≈473 nm, which nearly matches the bandgap energy at room temperature (2.61 eV, 475 nm).[27] Shi *et al.* also reported an emission peak at 473 nm for single crystals and assigned this peak to band edge emission.[28]

Films, powders, and ≈6 nm NCs dispersed in ethanol, like single crystals, luminesce between 468 nm and 478 nm.[27-31] Interestingly, in some cases, thin films cast from colloidal particles and annealed in Br_2 show fine structure reminiscent of phonon replicas (Fig. 1).[30] The intensities of these replicas and their resolution improve with annealing in Br_2. The spacing of the peaks varies but is frequently ≈25 meV (~200 cm^{-1}), nearly the same as the most intense Raman scattering at 190 cm^{-1} in $Cs_3Bi_2Br_9$ (Bi-Br stretching mode).[32,33] Interpreting this fine structure as phonon replicas and relying on their DFT

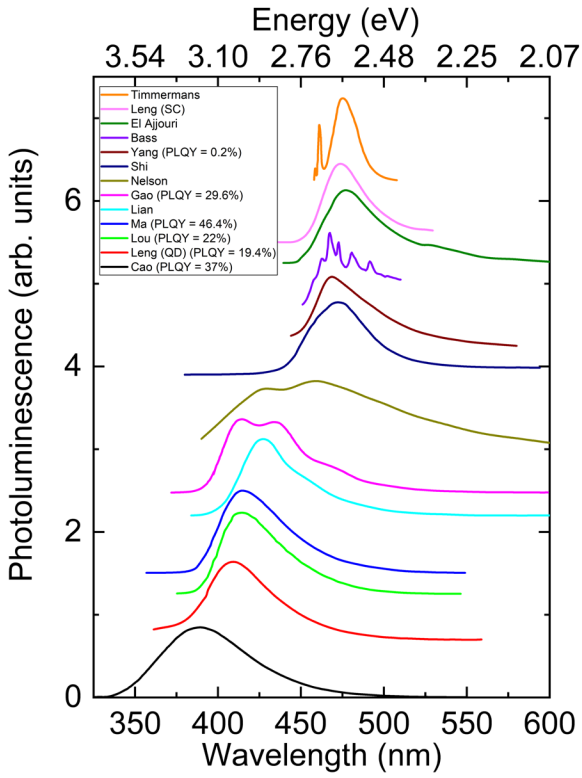

Fig. 1 Reported $Cs_3Bi_2Br_9$ PL from the literature. The curves are extracted from plots published in respective references *via* digitization using WebPlotDigitizer. Legend abbreviations are QD: quantum dots; SC: single crystals. Data are from Timmermans and Blasse,[16,17] Leng *et al.*,[27] Shi *et al.*,[28] El Ajjouri *et al.*,[29] Bass *et al.*,[30] Yang *et al.*,[31] Lou *et al.*,[35] Gao *et al.*,[36] Cao *et al.*,[37] Ma *et al.*,[38] Nelson *et al.*,[39] and Lian *et al.*.[40] Data are offset for clarity.

calculations that yielded an indirect bandgap, Bass *et al.* concluded that the emission is from an indirect bandgap rather than a direct bandgap. However, strong electron-phonon coupling in ionic semiconductors *via* the Frohlich interaction can also give rise to these peaks even if the bandgap is direct (*e.g.*, AlN).[34] Amongst these publications, only Yang *et al.* reported PLQY, 0.2% for ligand-free $Cs_3Bi_2Br_9$ nanocrystals, and 4.5% when oleic acid was used in the synthesis to cap the ≈5-6 nm diameter nanocrystals.[31] With oleic acid, the PL peak shifted from 468 to 460 nm.

In contrast to the above reports where the PL peak location agrees with that in single crystals, multiple publications reported PL significantly blue-shifted to wavelengths between 446 and 389 nm (See Table S1).[27,35-41] For instance, Lian *et al.* reported an emission peak at 427 nm for ≈9 nm thick and 60-250 nm long NCs, while Gao *et al.* reported broad overlapping peaks at 414 and 433 nm for ~10 nm NCs.[36,40] For ≈4 nm NCs, Leng *et al.* and Lou *et al.* reported PL peaks at 410 and 414 nm, respectively.[27,35] These authors attributed this shift to quantum confinement of excitons, but this assertion is not in agreement with PL from ≈6 nm NCs emitting at ≈468 nm, a size that falls between 4 and 10 nm.[31] (See also Table S1 for lack of blue-shift trends with size.)

Cao *et al.* reported an emission peak for ~5 nm NCs, which is even more blue-shifted to 389 nm.[37] Smaller, 3.3 nm NCs were reported by Ding *et al.*, but their emission peak is red-shifted

with respect to the 5 nm NCs to 446 nm.[41] Ma *et al.* showed an emission peak at 415 nm for the $Cs_3Bi_2Br_9$/BiOBr nanocomposites, which do not have well-defined shapes but have almost the same emission as the ≈4 nm NCs synthesized by Lou *et al.*[35,38] Interestingly, compared to the reports of PL peaks in the 468 to 478 nm range, the PLQY from blue-shifted emissions are significantly higher, reaching 46.4% (Fig. 1), the highest value, reported by Ma *et al.*

Nelson *et al.* also reported blue-shifted PL from NC dispersions, peaking at 427 nm and 460 nm (Fig. 1) but were commendably cautious and hesitant to assign it to quantum confinement.[39] They showed that the emission was identical to that from $BiBr_3$ solutions, raising the strong possibility that these blue-shifted emissions originate from precursors used in the synthesis and contaminating the product NC dispersions. Herein, we confirm their conclusion (*vide infra*).

The differences in reported PL peak wavelengths and PLQY of $Cs_3Bi_2Br_9$ raise doubts about blue-shifted emission peaks' origin and interpretation. Specifically, whether these shifts are due to quantum confinement in $Cs_3Bi_2Br_9$ NCs or emissions from unreacted precursors and impurities remains an open question. Here we settle this open question and show that high PLQY emissions attributed to quantum confinement in NCs originate from impurities. We recently resolved a similar discrepancy in the literature on optical absorption of $Cs_3Bi_2Br_9$ by showing that $[BiBr_6]^{3-}$ octahedra in solution absorb at ≈383 nm, and these absorptions may be misinterpreted as originating from the $Cs_3Bi_2Br_9$.[14] Herein, we show that $[BiBr_6]^{3-}$ and Bi complexes in solution emit efficiently (PLQY≈10%) in the 390-440 nm range. These emissions may also be misinterpreted as originating from NCs and quantum confinement. Using PVD, we avoid emissions from impurities and obtain PL from $Cs_3Bi_2Br_9$ thin films at 472 nm consistent with reported emission from single crystals, films, and ≈6 nm NCs dispersed in ethanol.[27-31] In fact, all PL that is consistent with single crystals and peaking at ≈468-478 nm range show low PLQY with the highest value of 0.2% for ligand-free $Cs_3Bi_2Br_9$ NCs reported by Yang *et al.*[31]

Experimental Section

Formation of bismuth bromide complexes in solution.
5-10 mg $BiBr_3$ (99%, Sigma Aldrich) and 5 ml oleic acid (90%, Alfa Aesar) were added to 5 ml of DMSO (99%, Sigma Aldrich) or 5 ml hexane (ACS Grade, VWR). 5-10 mg of $BiBr_3$ was also added to a mixture of 1 ml of oleic acid and 10 ml of toluene (ACS Grade, Pharmco-Aaper). Three resulting solutions were stirred and heated at 40 °C for 5 minutes. 5-10 mg of $BiBr_3$ was added to a mixture of 2 ml of DMSO, 2 ml of oleic acid (OA), and 20 ml of ethanol (Reagent alcohol, anhydrous, Sigma Aldrich). This solution was heated at 80 °C for 5 minutes. Photoluminescence from each solution was measured with QuantaMaster-8075-21 spectrophotometer (Horiba). PL was excited at a specific wavelength (5 nm bandwidth) depending on the sample, with double monochromator filtered emission from a Xe-arc lamp and detected using a red-extended Hamamatsu R13456 PMT.

Thin film deposition.
Films were deposited in a glove-boxed PVD system (Angstrom Engineering) with six evaporation sources. The five precursors, $BiBr_3$ (99%, Alfa Aesar), BiI_3 (99.999%, Alfa Aesar), CsBr (99.9%, Acros Organics), $YbBr_3$ (hydrate, 99.99%, Alfa Aesar), and CsI (99.998%, Alfa Aesar), were loaded into separate RADAK sources and baked overnight at 60, 60, 100, 110, and 100°C, respectively. $BiBr_3$ and BiI_3 were loaded in quartz ampoules, while the others were loaded in alumina ampoules. The precursors were co-evaporated onto glass substrates (25 × 25 mm^2) maintained at 30°C. The glass substrates were cleaned by sonicating in a 1:1 solution by volume of acetone (ACS Grade, VWR) and isopropanol (99.5%, VWR) for 30 minutes, dried in an oven, and cleaned with O_2 plasma for 30 minutes using Expanded Plasma Cleaner PDC-001-HP (Harrick Plasma) before loading them onto the substrate holder. Each precursor's evaporation rate was monitored during the deposition by separate quartz crystal microbalances (QCMs). The tooling factors were determined by evaporating CsBr and $BiBr_3$ separately and obtaining the film thickness from interference fringes in optical transmission. The tooling factors, the ratio of the deposition rate at the substrate to the deposition rate at the QCM expressed as %, were 39.7 and 42.9 for CsBr and $BiBr_3$, respectively. The tooling factor of CsBr was also used for CsI, $YbBr_3$, and BiI_3. During the deposition of $Cs_3Bi_2Br_9$ films, CsBr and $BiBr_3$ evaporation rates were controlled with a closed feedback loop at 1.15 Å/s and 1.36 Å/s, respectively. With these deposition rates, the ratio of CsBr molar flux to $BiBr_3$ molar flux is 2.8:2. The CsBr and $BiBr_3$ source temperatures were the manipulated variables to keep the evaporation rates constant but were ≈560 °C and ≈150 °C, respectively. For Yb-doped $Cs_3Bi_2Br_9$ films, CsBr, and $BiBr_3$, the evaporation rates were kept constant at 1.15 Å/s and 1.36 Å/s, respectively, while the $YbBr_3$ evaporation rate was varied from 0.14 to 0.70 Å/s, to change the amount of Yb doping. The $YbBr_3$ source temperature ranged from 680 to 740°C, depending on the evaporation rate and precursor amount in the ampoule. During the deposition of Yb-doped $Cs_3Bi_2(Br_{1-x}I_x)_9$ films ($0 \le x \le 0.26$), the evaporation rates of $BiBr_3$ and $YbBr_3$ were kept constant at 1.36 and 0.42 Å/s, respectively. The CsBr evaporation rate was reduced from 0.63 to 0 Å/s, while the CsI evaporation rate was increased from 0.63 to 1.38 Å/s to change x. The CsI temperature source rose from 510 to 570 °C as the evaporate rate increased. For x= 0.34, BiI_3 was used instead of CsI. $BiBr_3$, CsBr, and $YbBr_3$ were deposited at the rate of 0.54, 1.15, and 0.42 Å/s, respectively. BiI_3 deposition rate was 1.06 Å/s, with a corresponding temperature of ≈285 °C. The system's base pressure was 2×10^{-8} Torr, while the chamber pressure rose to ≈10^{-6} Torr during the deposition. Films were deposited for 30 minutes, resulting in 450±10 nm thick films for $Cs_3Bi_2Br_9$ and a deposition rate of 2.6 Å/s. All films were annealed on a hot plate at 300 °C for one hour in the glovebox.

Thin film characterization.
All films were characterized under ambient conditions at room temperature. PL spectra were measured using a QuantaMaster-8075-21 (Horiba) spectrophotometer. Visible PL from all films

was excited at 420 nm (5 nm bandwidth) with double monochromator filtered emission from a Xe-arc lamp and detected using a PMT detector. Near-infrared PL was excited at 360 nm and 420 nm for cesium bismuth bromide and mixed halide films, respectively. NIR PL was detected using liquid nitrogen cooled InGaAs detector. PLQY was measured using an integrating sphere (Quanta-Phi, Horiba), and the lamp power was measured using Power Meter 843-R and 818-UV photodetector (Newport). Details of the PLQY measurements are in the Supplementary Information. X-ray diffraction (XRD) patterns from the films were recorded using a Bruker D8 Discover General Area Detector Diffraction System (GADDS) equipped with a Cu-Kα source. Raman spectra were acquired using a Thermo Scientific DXR Raman microscope. Thin films were excited with a 785 nm laser, and Raman scattering in the range of 50-1800 cm^{-1} was collected with a 50× Olympus objective, dispersed using a high resolution (2 cm^{-1}) grating, and detected with a CCD detector. Films were examined using a Merlin field emission scanning electron microscope (Carl Zeiss, 5 kV, 110 pA). Their average composition over an area of approximately 10 μm^2 was determined using energy-dispersive X-ray spectroscopy (Oxford Instruments EDS) and vendor-provided sensitivity factors. Optical absorptions of the films were recorded using an Agilent Cary 5000 UV-Vis-NIR in the 200-2000 nm range. Thin-film interference fringes below the bandgap energy (>500 nm) were used to determine the film thicknesses as described previously.[14]

Results and discussion

Photoluminescence from bismuth bromide solutions

When visible PL from $Cs_3Bi_2Br_9$ NC dispersions is measured, the emission can originate from NCs, unreacted precursors, ligands, or impurities in the solution. Bismuth cations form octahedral or tetrahedral complexes with anions (*e.g.,* Br^-), ligands, and polar solvent molecules in the solution. These complexes emit in the 390 nm to 436 nm range with wavelength depending on the ligand field. For instance, Fig. 2 shows PL from $BiBr_3$ and the common ligand oleic acid (OA) in different solvents peaking in this wavelength range. Troublingly, the peak locations and linewidths of these emissions match those reported for $Cs_3Bi_2Br_9$ NC dispersions even though the solutions in Fig. 2 do not contain any NCs.[27,35,36,38,40] For instance, $BiBr_3$ in oleic acid, ethanol, and DMSO emits at 410 nm when excited at 330 nm, which matches with the emission peak assigned to $Cs_3Bi_2Br_9$ NCs by Leng *et al.*,[27] who prepared their NCs in oleic acid, ethanol, and DMSO and excited the dispersions at 330 nm. Fig. S1a in the Supplementary Information shows that normalized PL from Leng *et al.* can be reproduced with PL from $BiBr_3$ in ethanol, oleic acid, and DMSO. Small changes to excitation wavelength or the solution composition shift the emission peak slightly (≈10 nm, see Fig. S2), but these emissions from bismuth complexes remain robust. Using the reported excitation wavelengths, solvents, and ligands, we could reproduce emissions between 390 nm to 436 nm assigned to $Cs_3Bi_2Br_9$ NCs in half a dozen articles: our solutions did not contain any $Cs_3Bi_2Br_9$ NCs. (Please do see Supplementary Information Fig. S1.)

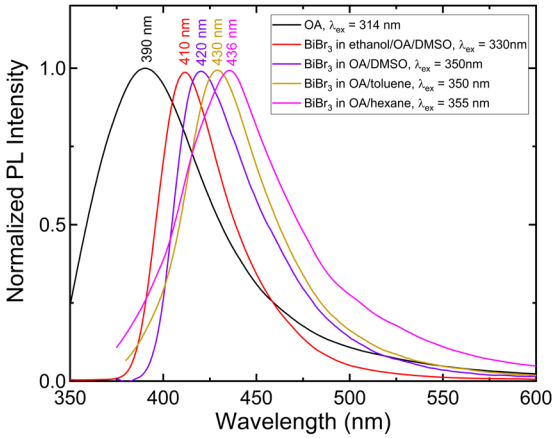

Fig. 2 Photoluminescence from oleic acid (OA) and bismuth bromide in different solvents. DMSO is dimethyl sulfoxide. The peak emission wavelengths at the excitation wavelength, λ_{ex}, are shown.

High PLQY values accompanied these reports of emissions in the 390-436 nm range. For instance, Lou *et al.* and Ma *et al.* reported PLQYs of 22% (at 414 nm) and 46.4% (at 415 nm), respectively, and assigned them to $Cs_3Bi_2Br_9$ NCs.[35,38] We excited $BiBr_3$ in oleic acid and DMSO at 325 nm and measured a PLQY of 9.5% at 415 nm, the same wavelength as Lou *et al.* and Ma *et al.,* but without any $Cs_3Bi_2Br_9$ NCs in our solutions. Notably, both studies used oleic acid and DMSO for preparing their dispersions, raising the possibility that these emissions assigned to NCs dispersed in DMSO with oleic acid originate from the unreacted Bi precursors (complexes) present in the dispersion, rather than the $Cs_3Bi_2Br_9$ NCs. Lou *et al.* found that the $Cs_3Bi_2Br_9$ NCs prepared without ligands exhibited a weak 468 nm PL, but the dispersion prepared with oleic acid ligands emitted 414 nm PL with 22% PLQY.[35] While they attributed this increase to passivation of defects by the ligands, an alternative explanation is the formation of strongly luminescent bismuth complexes emitting at 414 nm from the excess $BiBr_3$ precursor and oleic acid in DMSO, as shown in Fig. 2, Fig. S1, and Fig. S2.

To add to the possible sources of PL artifacts, oleic acid, a ligand commonly used in the synthesis of $Cs_3Bi_2Br_9$ NCs, itself emits strongly at 390 nm when excited at 314 nm (Fig. 2). For OA, we measured a PLQY of ≈5-12%, but this value depends on the excitation wavelength and may depend on OA's source and even the production lot. This peak and its line shape match the emission reported by Cao *et al.* (37% PLQY), who assigned it to $Cs_3Bi_2Br_9$ NCs.[37] The OA PL is excitation dependent and peaks between 380-420 nm (Fig. S3).

In summary, we could obtain the same emission peaks, reported between 390 nm to 436 nm and attributed to $Cs_3Bi_2Br_9$ NCs, from $BiBr_3$ and OA solutions that do not contain any $Cs_3Bi_2Br_9$ NCs. All publications that reported PL in the 390 nm to 436 nm range used OA or $BiBr_3$ or both, raising the possibility of contamination even when caution is exercised to clean the NC product. Thus, our comparisons raise doubts about the origin of the reported $Cs_3Bi_2Br_9$ PL between 390 nm to 436 nm and the high value of the PLQY (as high as 46.4%).[38] These emissions likely originate from the unreacted precursors and ligands present in the solutions.

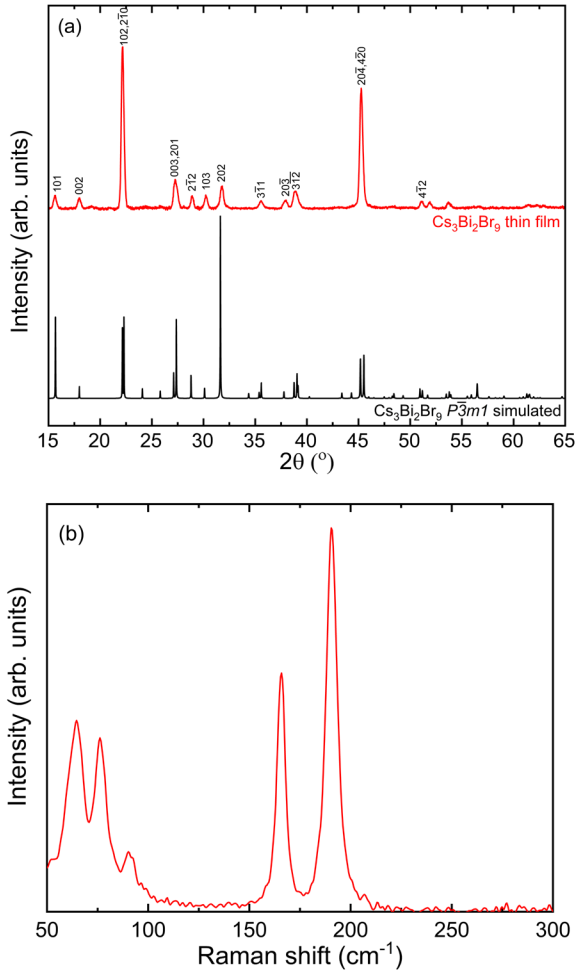

Fig. 3 (a) XRD patterns of $Cs_3Bi_2Br_9$ film compared to the simulated powder diffraction pattern (offset for clarity). (b) Raman spectrum of $Cs_3Bi_2Br_9$ film.

Below we confirm the studies that reported $Cs_3Bi_2Br_9$ PL between 468 nm and 478 nm, albeit with very low PLQY. We study the optical properties of $Cs_3Bi_2Br_9$ films deposited *via* co-evaporation of CsBr and $BiBr_3$ with a ≈3:2 (CsBr:$BiBr_3$) molar ratio. PVD avoids the solution phase and eliminates the possibility of spurious PL originating from unreacted precursors and ligands.

Photoluminescence from $Cs_3Bi_2Br_9$ thin films

Figure 3a shows an XRD pattern from a $Cs_3Bi_2Br_9$ film deposited using PVD, which matches the pattern simulated using the single-crystal structure reported by Lazarini.[18] $BiBr_3$ and CsBr diffraction peaks are absent, suggesting that the two precursors reacted completely to form $Cs_3Bi_2Br_9$. The $Cs_3Bi_2Br_9$ film exhibits two signature Raman peaks at 191 and 166 cm^{-1}, corresponding to A_{1g} and E_g normal modes of Bi-Br vibrations in the corner-sharing $[BiBr_6]^{3-}$ octahedra, confirming that the film is trigonal $Cs_3Bi_2Br_9$ (Fig. 3b).[32,33] This $Cs_3Bi_2Br_9$ film exhibits an absorption peak at 433 nm with an onset at 470 nm (Fig. 4). The absorption drops as wavelength decrease from the peak at 433 nm but starts rising again at ≈380 nm. The bandgap energy determined from the Tauc plot is 2.6 eV, consistent with previous reports

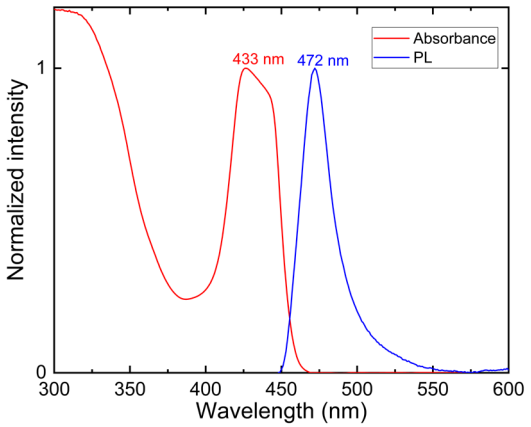

Fig. 4 Absorbance and photoluminescence of a $Cs_3Bi_2Br_9$ thin film. Excitation wavelength for PL is 420 nm. Thin film interference fringes were subtracted from the absorbance.

and single-crystal absorption measurements.[28,30] DFT calculations reveal that the states near the valence band maximum comprise Bi 6s and Br 4p orbitals, while the bottom of the conduction band is made mainly of Bi 6p orbitals.[29] We associate the absorption peak at 433 nm with the excitation of a localized exciton, with large binding energy, on $[BiBr_6]^{3-}$ octahedra which interact weakly with each other in the $Cs_3Bi_2Br_9$ perovskite structure.

When excited at 420 nm, $Cs_3Bi_2Br_9$ film emits at 472 nm (Fig. 4), with a long tail that persists up to 600 nm and a Stoke shift of 39 nm compared to the absorption peak at 433 nm. This PL is the same as that reported by Timmermans and Blasse[17] and attributed to recombination on defect centers hypothesized to be Bi^{3+} on disordered sites. The location of this emission agrees with the PL reported for $Cs_3Bi_2Br_9$ single crystals, some of the reports for NCs, and powders. The highest reported PLQY of $Cs_3Bi_2Br_9$ at this wavelength range is 0.2%, with the maxima at 468 nm for NCs.[31] While we could detect PL in our spectrometer, we could not detect $Cs_3Bi_2Br_9$ emission inside an integrating sphere to measure PLQY at this wavelength from our films due to nonradiative relaxation and reabsorption. We attribute the long PL tail to excitons trapped on defects. Such a tail has been observed in nearly all measurements, including single crystals, and is hypothesized to be due to excitons trapped and localized by Bi^{3+} cation disorder. Emission from $Cs_3Bi_2Br_9$ reflects multiple times in the integrating sphere and is reabsorbed, eventually creating trapped excitons that decay nonradiatively or radiatively at longer wavelengths.

Yb-doped $Cs_3Bi_2Br_9$ thin films

We deposited Yb-doped $Cs_3Bi_2Br_9$ films via co-evaporation of CsBr, $BiBr_3$, and $YbBr_3$ and varied the $YbBr_3$ evaporation rate to change the Yb concentration. While we use the term doping, significantly higher Yb concentrations than typical dopant concentrations can be incorporated into $Cs_3Bi_2Br_9$. We hypothesize that Yb^{3+} ions would substitute Bi^{3+} ions in the crystal structure to form $Cs_3Bi_{2-x}Yb_xBr_9$ because they are isovalent. However, $Cs_3Bi_{2-x}Yb_xBr_9$ solid solution is unlikely for the entire composition range from x=0 to x=2 because ionic radii

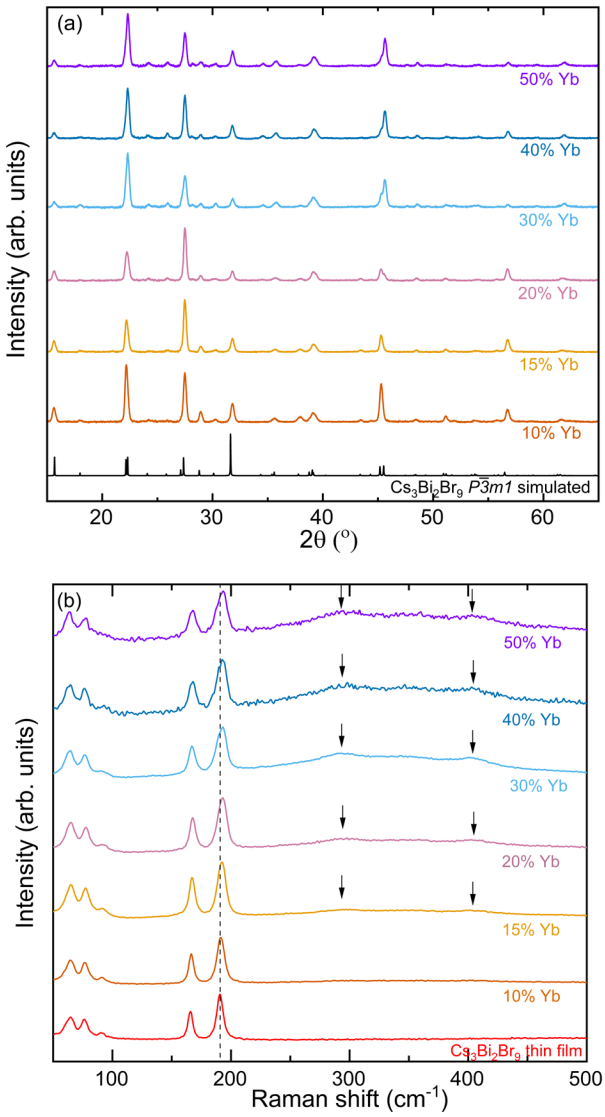

Fig. 5 (a) XRD patterns of Yb-doped $Cs_3Bi_2Br_9$ films compared to the simulated undoped $Cs_3Bi_2Br_9$ powder diffraction pattern. (b) Raman spectra of Yb-doped $Cs_3Bi_2Br_9$ and undoped $Cs_3Bi_2Br_9$ films. The dotted line guides the eye to make the Raman peak shift and broadening upon Yb incorporation more obvious. Data offset for clarity.

of Yb^{3+} and Bi^{3+} are 101 pm and 117 pm, respectively, and the stable $Cs_3Bi_2Br_9$ and $Cs_3Yb_2Br_9$ crystal structures have different symmetries, $P\bar{3}m1$ and $R\bar{3}c$, respectively.[42,43] The $[BiBr_6]^{3-}$ octahedra in $Cs_3Bi_2Br_9$ are connected corner-to-corner, while the $[YbBr_6]^{3-}$ octahedra in $Cs_3Yb_2Br_9$ are connected face-to-face. In this article, we report the nominal Yb^{3+} concentration expressed as a percent of the Bi^{3+} ions (*i.e.,* 100 × (x/(2-x) %) as determined from the $BiBr_3$ and $YbBr_3$ fluxes measured using the QCMs.

Fig. 5a shows XRD patterns from Yb-doped $Cs_3Bi_2Br_9$ films with Yb concentrations from 0 to 50%. All XRD peaks of each film match with the $Cs_3Bi_2Br_9$ single-crystal XRD pattern, suggesting that all Yb-doped films (up to at least 50% Yb) crystallize with the trigonal structure $(P\bar{3}m1, \#164)$. We do not observe any significant XRD peak shifts or peak broadening with increasing Yb concentration: any change in the lattice

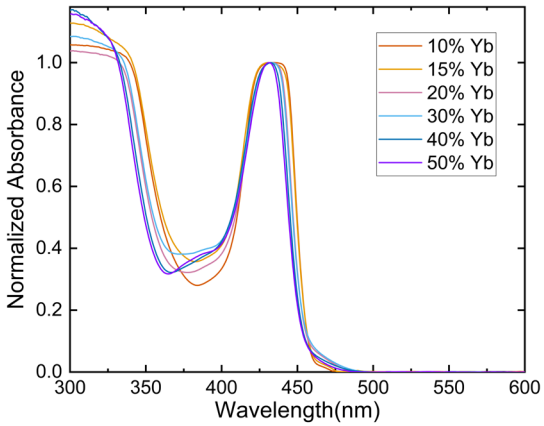

Fig. 6 Optical absorbance of Yb-doped $Cs_3Bi_2Br_9$ film. Absorbance is normalized to the peak value at ≈472 nm to show the slight blue-shift. All film thicknesses were within 10 nm of each other (450±10 nm).

parameters may be too small to be observed in our XRD measurements. Moreover, XRD peaks are broadened due to the Scherrer effect, making small shifts in XRD peaks more challenging to detect. In contrast, Raman peaks at 166 and 191 cm^{-1} shift to 168 and 193 cm^{-1}, respectively, as Yb concentration increases from 0 to 50% (Fig. 5b). The line shape of the peak at 193 cm^{-1} becomes noticeably asymmetric and broadens in films with 20% Yb and greater. Raman peak broadening and shifting to higher wavenumbers may indicate the substitution of Bi^{3+} with Yb^{3+} in the crystal structure. Yb presence in neighboring octahedra will perturb the Bi-Br bonds and introduce heterogeneities in Bi-Br bond lengths, accounting for the shift and the broadening. Additionally, two weak peaks at 290 and 400 cm^{-1} (arrows in Fig. 5b) become strong enough to be detected and appear in films with 15% Yb and grow as Yb concentration increases further. Since they are not present in $Cs_3Bi_2Br_9$ films without Yb, we assign these two features to Yb-Br vibrations.

We could detect Yb presence in the films with EDS, and the concentrations determined from EDS measurements increased monotonically with increasing $YbBr_3$ evaporation rate and the nominal Yb concentration (Supplementary Information Table S2). Accurate quantitative measurement using EDS is difficult, however, because Yb and Br peaks overlap.

Fig. 6 shows that Yb doping does not change the absorption of $Cs_3Bi_2Br_9$ films significantly. The absorption peak at 433 nm for undoped films blue shifts slightly to 431 nm for films with 50% Yb. This small change is consistent with the conclusion that the $Cs_3Bi_2Br_9$ structure is maintained up to 50% Yb incorporation. Slightly blue-shifted absorption in films with Yb incorporation can result from tiny lattice contractions when smaller Yb replaces Bi in $[BiBr_6]^{3-}$ octahedra that were too small to detect using XRD but noticeable in more sensitive optical absorption. Notably, there is a weak absorption feature at ≈383 nm for $Cs_3Bi_2Br_9$ films with 30-50% Yb and absorption in this region is generally higher for films with increasing Yb concentration. Previously we showed that isolated $[BiBr_6]^{3-}$ octahedra that do not share corners with others absorb at 383 nm.[14] Based on this, we hypothesize that the absorption around

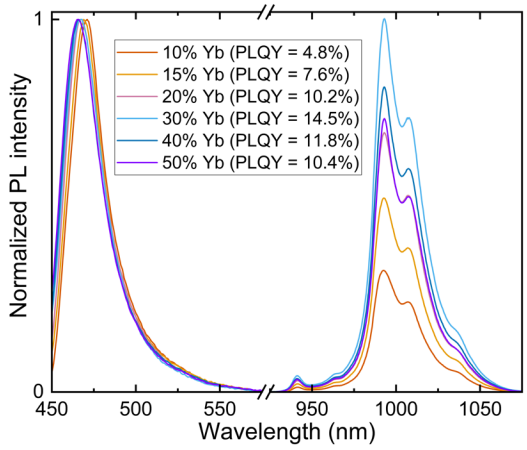

Fig. 7 Normalized visible and NIR PL from Yb-doped $Cs_3Bi_2Br_9$ films. Visible PL is normalized to the peak value for each Yb concentration. NIR PL is normalized with the peak value for the film with 30% Yb and scaled with the PLQY values for other films. PLQY is calculated as the integrated number of photons emitted in the NIR region (900-1100 nm) over the number of photons absorbed at the excitation wavelength (360 nm, 5 nm bandwidth.) See Supplementary Information for details of PLQY determination. The excitation wavelength is 420 and 360 nm for visible and NIR emissions, respectively.

383 nm could be a sign of $[BiBr_6]^{3-}$ octahedra not connected to others and formed from excess Bi^{3+} displaced by Yb^{3+}. While most of the excess Bi^{3+} is expected to desorb as $BiBr_3$ during annealing, some can remain on the internal surfaces, such as the grain boundaries. A drawback of PVD in synthesizing cesium bismuth bromide is the potential presence of excess $BiBr_3$ in the films when ytterbium replaces bismuth ions. Post-annealing treatment and reducing $BiBr_3$ flux may help mitigate this problem.

Fig. 7 shows visible and NIR emissions from Yb-doped $Cs_3Bi_2Br_9$ films. When excited at 420 nm, all Yb-doped $Cs_3Bi_2Br_9$ films exhibit broad visible emission with long tails that persist to 600 nm. The visible emission from the film doped with Yb shows a small but systematic blue shift from 472 nm for films with no Yb to 465 nm for films with 50% Yb. This shift is consistent with absorption in these films, which also shifts to higher energies with increasing Yb concentration. As was the case with $Cs_3Bi_2Br_9$ films without Yb, we do not detect visible PL from these films in the integrating sphere. Reabsorption eventually channels the energy to trapped excitons that decay nonradiatively or radiatively but at a different wavelength. Visible emissions of Yb-doped $Cs_3Bi_2Br_9$ are too weak to determine PLQY using the integrating sphere. Visible PL data (not normalized) measured outside the integrating sphere (Fig. S4) shows small nonsystematic intensity changes (±15%) among films with different amounts of Yb. We choose not to attribute these to systematic changes with Yb concentration and draw any conclusions from these variations because of the sample-to-sample variations in scattering, excitation coupling to the film, angle of detection, and shifts in background.

All Yb-doped $Cs_3Bi_2Br_9$ films exhibit NIR emissions which share the same features: a weak peak at 941 nm, a strong peak at 993 with a shoulder at 964 nm, and another strong peak at 1008 nm with a shoulder at 1036 nm (Fig. 7). These peaks

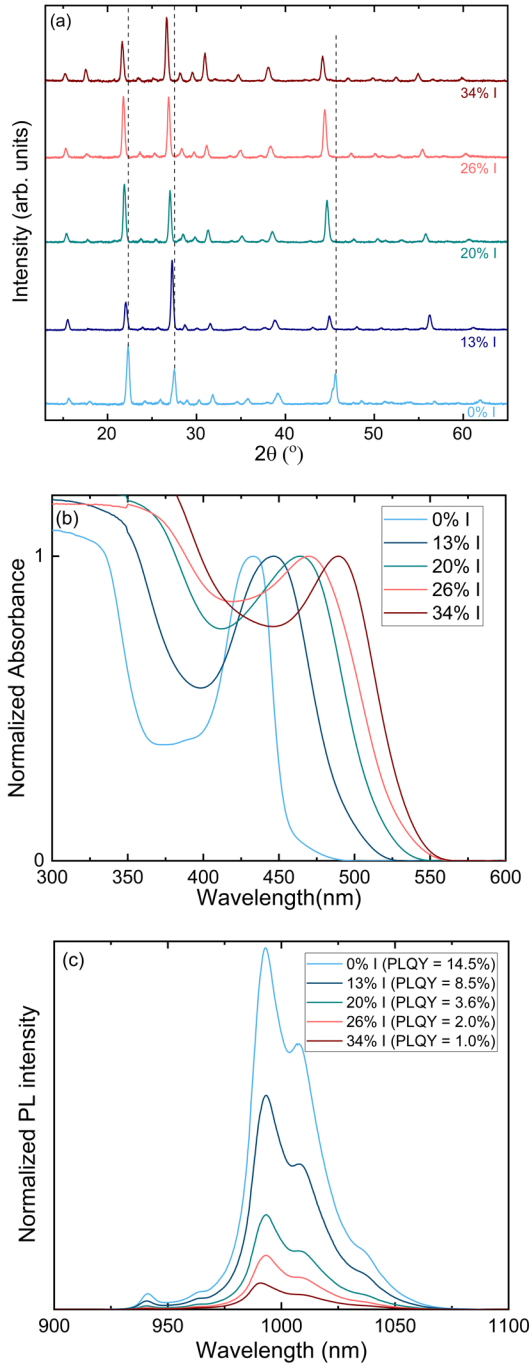

Fig. 8 (a) XRD patterns (offset for clarity), (b) absorbance and (c) NIR photoluminescence of 30% Yb-doped $Cs_3Bi_2(Br_{1-y}I_y)_9$ films. Thin film interference fringes were subtracted from the absorbance. NIR emission is excited with 420 nm light. Absorbance is normalized with the maximum value of the excitonic peak for each film. NIR PL is normalized with the peak value for the film with 30% Yb and 0% I and scaled with the PLQY values for other films.

correspond to Yb^{3+} $^2F_{5/2} \rightarrow {}^2F_{7/2}$ electronic transitions. Multiple peaks result from crystal field splitting of the Yb^{3+} *f* orbitals into multiple levels, leading to electronic transitions with different energies. NIR PLQY, the integrated number of photons emitted via the $^2F_{5/2} \rightarrow {}^2F_{7/2}$ transition (900-1100 nm) divided by the number of photons absorbed at the excitation wavelength (360

nm, 5 nm bandwidth), increases with Yb concentration up to 30% Yb and then decreases. (See Supplementary Information for details of PLQY determination). The film doped with 30% Yb has the highest PLQY, 14.5%. 14.5% PLQY is remarkable since the $Cs_3Bi_2Br_9$ films without Yb do not emit efficiently in the visible, and almost all excitons relax nonradiatively. Doping with Yb introduces a mechanism for energy transfer, from the $Cs_3Bi_2Br_9$ to Yb^{3+}, which competes effectively with nonradiative relaxation culminating in 14.5% PLQY. Increasing Yb concentration from 10% to 30% improves the PLQY from 4.8% to 14.5%. However, PLQY decreases to 10.4% when the Yb concentration is 50%. One explanation is that increasing Yb concentration beyond 30% increases the concentration of nonradiative trapping sites. Increasing the annealing time from 1 hour to 2 hours at 300°C does not increase the PLQY of the film doped with 30% Yb. Increasing the annealing temperature further to 350°C and annealing at that temperature for 1 hour quenches the NIR emission, consistent with reports that $Cs_3Bi_2Br_9$ decomposes at ≈350°C.[44]

Yb-doped $Cs_3Bi_2(Br_{1-y}I_y)_9$ films

Fast quantum cutting was recently found to be a reason for high PLQY in Yb-doped $CsPbCl_xBr_{3-x}$ (x>2) nanocrystals. In these NCs, PLQY is as high as 190% but decreases rapidly when the Br concentration is increased above approximately x<2 such that the bandgap energy of the $CsPbCl_xBr_{3-x}$ is less than twice the Yb^{3+} $^2F_{5/2}\rightarrow$ $^2F_{7/2}$ transition. Keeping Yb concentration at 30%, we red-shifted the $Cs_3Bi_2Br_9$ films' bandgap by adding iodine and measured the PLQY as a function of % iodine and the bandgap energy. We deposited Yb-doped $Cs_3Bi_2(Br_{1-y}I_y)_9$ films (0≤y≤0.34) by coevaporating CsBr, $BiBr_3$, $YbBr_3$, and CsI or BiI_3. The halide composition was determined from the QCM rates. XRD diffraction (Fig. 8a) showed that all $Cs_3Bi_2(Br_{1-y}I_y)_9$ films (0≤y≤0.34) crystallized in the trigonal structure $(P\bar{3}m1, \#164)$ with diffraction peaks shifting to lower 2θ values as the amount of iodide (y) increases. Such shifts are consistent with the expected expansion of the crystal lattice as larger I^- substitutes for Br^-. The absorption peak is red-shifted from 433 nm for y=0 to 490 nm for y=0.34 (Fig. 8b). This shift results from a decrease in the bandgap when iodide ions replace bromide ions and expand the crystal structure. We surmise that the absorption peak widths increase for films with iodide because of band edge fluctuations. Bromide and iodide ions are not mixed at the exact ratio of (1-y):y throughout the entire film, so bandgap fluctuations, due to local halogen concentration fluctuations, can broaden the absorption peaks. The absorption onset for the $Cs_3Bi_2(Br_{1-y}I_y)_9$ film with y=0.34 and 30% Yb is at 570 nm (2.2 eV), so its bandgap is smaller than twice the electronic transition of Yb^{3+} $^2F_{5/2}\rightarrow$ $^2F_{7/2}$ (~1000 nm), which should prohibit the quantum cutting process. While visible emission was not detected from $Cs_3Bi_2(Br_{1-y}I_y)_9$ films doped with 30% Yb, these films exhibit the same emission features in the NIR region as the films without iodide (Fig. 8c) when excited at 420 nm but with sharply decreasing PLQY as y increases. The similarities in NIR emission features suggest that Yb^{3+} emission centres have the same surrounding ligand field in $Cs_3Bi_2(Br_{1-y}I_y)_9$ films. One hypothesis for decreasing PLQY with y is that the introduction of iodine increases the nonradiative relaxation rate relative to energy transfer to the Yb^{3+} centres. This hypothesis would also explain the quenching of the visible PL upon iodine substitution. Another hypothesis is that the energy transfers to Yb^{3+} via quantum cutting, but the narrower bandgap prohibits NIR emission by this mechanism. This scenario would suggest that while we do not reach PLQY >100%, quantum cutting still happens in our Yb-doped $Cs_3Bi_2Br_9$ films with 14.5% PLQY. As the bandgap decreases with y, the PLQY decreases to 1% at y=0.34. The increasing width of the absorption peak suggests the presence of local halogen concentration and bandgap fluctuations so that NIR PL is not entirely extinguished when the absorption onset is reduced below 2.5 eV.

Another evidence for the quantum cutting is the fast energy transfer from $Cs_3Bi_2Br_9$ to Yb^{3+}. This energy transfer competes efficiently both with visible radiative decay and with nonradiative decay. The radiative decay happens in less than 1 ns, the limit of our time-correlated single-photon counting set up. The nonradiative decay happens in ≈2 ps in $Cs_3Bi_2Br_9$.[31] Using this value for nonradiative recombination time constant and the measured PLQY, we estimate that the energy transfer in $Cs_3Bi_2Br_9$ to Yb^{3+} occurs at least around 10-15 ps. Milstein *et al.* reported a time constant on the order of 1 ps for quantum cutting in Yb^{3+}-doped $CsPbCl_3$.[21] This raises the possibility that the fast energy transfer from $Cs_3Bi_2Br_9$ to Yb is via quantum cutting. NIR PLQY of 14.5% is indeed an encouraging value from $Cs_3Bi_2Br_9$, which may be a viable material for quantum cutting.

Conclusions

Photoluminescence from $Cs_3Bi_2Br_9$ thin films peaks at ≈472 nm. Using physical vapor deposition technique to deposit $Cs_3Bi_2Br_9$, we avoid emissions from undesired caesium bismuth bromide phases, excess precursors, ligands, and other impurities in common solvents, and we show that previously reported blue-shifted emissions in the 390-440 nm range from $Cs_3Bi_2Br_9$ NC dispersions likely originate from $BiBr_3$ and oleic acid in these dispersions and not from $Cs_3Bi_2Br_9$ NCs. Yb could be incorporated into the $Cs_3Bi_2Br_9$ films at high levels, and these films luminesced efficiently in the NIR (1.25 eV Yb^{3+} $^2F_{5/2}\rightarrow$ $^2F_{7/2}$ transition) with 14.5% PLQY. The NIR PLQY efficiency decreased sharply when the $Cs_3Bi_2(Br_{1-y}I_y)_9$ bandgap energy was decreased below twice the Yb^{3+} $^2F_{5/2}\rightarrow$ $^2F_{7/2}$ transition energy, raising the prospects of quantum cutting in this material.

Conflicts of interest

There are no conflicts to declare.

Acknowledgments

The X-ray microdiffractometer with GADDS was acquired through the support of the National Science Foundation under Award Numbers CRIF/CHE-0840277 and the NSF MRSEC Program under Award Number DMR-0820341.

References

1. L. Protesescu, S. Yakunin, M. I. Bodnarchuk, F. Krieg, R. Caputo, C. H. Hendon, R. X. Yang, A. Walsh and M.V. Kovalenko. *Nano Lett.,* 2015, **15**, 3692−3696.
2. A. Swarnkar, A. R. Marshall, E. M. Sanehira, B. D. Chernomordik, D. T. Moore, J. A. Christians, T. Chakrabarti and J. M. Luther. *Science*, 2016, **354**, 92-95.
3. J. Song, J. Li, X. Li, L. Xu, Y. Dong and H. Zeng. *Adv. Mater.*, 2015, **27**, 7162–7167.
4. T. Chiba, K. Hoshi, Y.J. Pu, Y. Takeda, Y. Hayashi, S. Ohisa, S. Kawata and J. Kido. *ACS Appl. Mater. Interfaces,* 2017, **9**, 18054−18060.
5. J. Li, L. Xu, T. Wang, J. Song, J. Chen, J. Xue, Y. Dong, B. Cai, Q. Shan, B. Han and H. Zeng. *Adv. Mater.*, 2017, **29**, 1603885.
6. P. Ramasamy, D.H. Lim, B. Kim, S.H. Lee, M.S Lee and J. S. Lee. *Chem. Commun*., 2016, **52**, 2067—2070.
7. H. Guan, S. Zhao, H. Wang, D. Yan, M. Wang and Z. Zang. *Nano Energy,* 2020, **67**,104279.
8. X. Liu, T. Xu, Y. Li, Z. Zang, X. Peng, H. Wei, W. Zha and F. Wang. *Solar Energy Materials and Solar Cells,* 2018, **187**, 249-254.
9. D. Yan, S. Zhao, H. Wang and Z. Zang. *Photonics Research,* 2020, **8-7**, 1086-1092.
10. H. Wang, H. Li, S. Cao, M. Wang, J. Chen and Z. Zang. *Sol. RRL,* 2020, **4**, 2000226.
11. B. W. Park, B. Philippe, X. Zhang, H. Rensmo, G. Boschloo and E. M. J. Johansson. *Adv. Mater*., 2015, **27**, 6806–6813.
12. J. Pal, A. Bhunia, S. Chakraborty, S. Manna, S. Das, A. Dewan, S. Datta and A. Nag. *J. Phys. Chem. C*., 2018, **122**, 10643-10649.
13. S. E. Creutz, H. Liu, M. E. Kaiser, X. Li and D. R. Gamelin. *Chem. Mater.,* 2019, **31**, 4685-4697.
14. M. N. Tran, I. J. Cleveland and E. S. Aydil. *J. Mater. Chem. C*., 2020, **8**, 10456-10463.
15. M. N Tran, I. J. Cleveland and E. S. Aydil. J*. Vac. Sci. Technol. A*, 2021, **39**, 013409.
16. C. W. M. Timmermans and G. Blasse. *J. Luminescence.,* 1981*,* **24-25**, 75-78.
17. C. W. M. Timmermans and G. Blasse. *Phys. Stat. Sol. (b),* 1981*,* **106**, 647-655.
18. F. Lazarini. *Acta Cryst*, 1977, **B33**, 2961-2964.
19. I. P. Aleksandrova, R. Burriel, J. Barolome, B. Sh. Bagautdinov, J. Blasco, A. A. Sukhovky, J. M. Torres, A. D. Vasiljev and L. A. Solovjev. *Phase Transitions*, 2002, **75**, 607–620.
20. G. Pan, X. Bai, D. Yang, X. Chen, P. Jing, S. Qu, L. Zhang, D. Zhou, J. Zhu, W. Xu, B. Dong and H. Song. *Nano Lett*., 2017, **17**, 8005-8011.
21. T. J. Milstein, D. M. Kroupa and D. R. Gamelin. *Nano Lett.,* 2018, **18**, 3792-3799.
22. D. M. Kroupa, J. Y. Roh, T. J. Milstein, S. E. Creutz and D. R. Gamelin. *ACS Energy Lett*., 2018, **3**, 2390-2395.
23. M. J. Crane, D. M. Kroupa, J. Y. Roh, R. Y. Anderson, M. D. Smith and D. R. Gamelin. *ACS Appl. Energy Mater*., 2019, **2**, 4560-4565.
24. S. Zhao, Y. Zhang and Z. Zang. *Chem. Commun*., 2020, **56**, 5811-5814.
25. W. Lee, S. Hong and S. Kim. *J. Phys. Chem. C,* 2019, **123**, 2665–2672.
26. Y. Mahor, W. J. Mir and A. Nag. *J. Phys. Chem. C*, 2019, **123**, 15787-15793.
27. M. Leng, Y. Yang, K. Zeng, Z. Chen, Z. Tan, S. Li, J. Li, B. Xu, D. Li, M. P. Hautzinger, Y. Fu, T. Zhai, L. Xu, G. Niu, S. Jin and J. Tang. *Adv. Funct. Mater.,* 2018, **28**, 1704446.
28. M. Shi, G. Li, W. Tian, S. Jin, X. Tao, Y. Jiang, E. A. Pidko, R. Li and C. Li. *Adv. Mater*., 2020, **32**, 2002137.
29. Y. El Ajjouri, V. S. Chirvony, N. Vassilyeva, M. Sessolo, F. Palazob and H. J. Bolink. *J. Mater. Chem. C*, 2019, **7**, 7236-7240.
30. K. K. Bass, L. Estergreen, N. C. Savory, J. Buckeridge, D. O. Scanlon, P. I. Djurovich, S. E. Bradforth, M. E. Thompson and B. C. Melot. *Inorg. Chem*., 2017, **56**, 42-45.
31. B. Yang, J. Chen, F. Hong, X. Mao, K. Zheng, S. Yang, Y. Li, T. Pullerits, W. Deng and K. Han. *Angew. Chem. Int. Ed*., 2017, **56**, 12471-12475.
32. G. Bator, J. Baran, R. Jakubas and M. Karbowia. *Vibrational Spectroscopy*, 1996, **18**, 11-20.
33. M. Y. Valakh, M. P. Lisitsa, E. Y. Peresh, O. V. Trylis and A. M. Yaremko. *J. Mol. Struct.*, 1997, **436-437**, 309-313.
34. A. Sedhain, J. Li, J. Y. Lin and H. X. Jiang. *Appl. Phys. Lett.,* 2009, **95**, 061106.
35. Y. Lou, M. Fang, J. Chen and Y. Zhao. *Chem. Commun*., 2018, **54**, 3779-3782.
36. M. Gao, C. Zhang, L. Lian, J. Guo, Y. Xia, F. Pan, X. Su, J. Zhang, H. Li and D. Zhang. *J. Mater. Chem. C.*, 2019, **7**, 3688-3695.
37. Y. Cao, Z. Zhang, L. Li, J. Zhang and J. Zhu. *Anal. Chem*., 2019, **91**, 8607-8614.
38. Z. Ma, Z. Shi, L. Wang, F. Zhang, D. Wu, D. Yang, X. Chen, Y. Zhang, C. Shan and Z. Li. *Nanoscale*, 2020, **12**, 3637-3645.
39. R. D. Nelson, K. Santra, K.; Y. Wang, A. Hadi, J.W. Petrich and M. G. Panthani, M.G. *Chem. Commun*., 2018, **54**, 3640-3643.
40. L. Lian, G. Zhai, F. Cheng, Y. Xia, M. Zheng, J. Ke, M. Gao, H. Liu, D. Zhang, L. Li, J. Gao, J. Tang and J. Zhang. *CrystEngComm*, 2018, **20**, 7473-7478.
41. N. Ding, D. Zhou, G. Pan, W. Xu, X. Chen, D. Li, X. Zhang, J. Zhu, Y. Ji and H. Song. *ACS Sustain. Chem. Eng.,* 2019, **7**, 8397-8404.
42. R. D. Shannon. *Acta Crystallogr A*, 1976, **32**, 751-767.
43. A. Donni, A. Furrer and H. U. Gudel. *J. Solid State Chem.*, 1989, **81**, 278-284.
44. S. V. Kun, E. Y. Peresh, V. B. Lazarev and A. V. Kun. *Izv. Akad. Nauk SSSR, Neorg. Mater.,* 1991, **27**, 611–615.